Modelling of Voltage Source Converter in Battery Energy Storage System for Voltage Support in the Distribution Grid

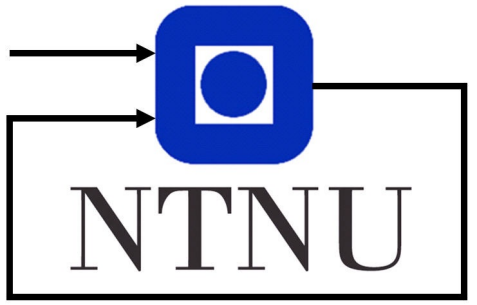

Author:
Vebjørn Wøllo

Supervisor:
Jon Are Suul

Specialization project
Department of Engineering Cybernetics
Norwegian University of Science and Technology

December 19, 2022

Preface

This report is written as the project thesis during my master's studies at Norwegian University of Science and Technology (NTNU). It has been written at the Faculty of Information Technology and Electrical Engineering, Department of Engineering Cybernetics. The project has been supervised by Professor Jon Are Suul and co-supervised by Jonatan Ralf Axel Klemets in cooperation with SINTEF Energy.

Abstract

The distribution grid is under increasing demand due to electrification and more distributed generation. This causes the power quality of the grid to suffer, and measures to alleviate this problem must be taken.

This project thesis investigates how a voltage source converter used in a battery energy storage system to be used for voltage support can be modelled and linearized into a linearized model. The necessary components of the battery energy storage system have been explained and the influence it has on the voltage of the distribution grid. Nonlinear and linear time-invariant systems have been described, and how a small-signal model of the system can be developed. A complete model of the differential equations of the inner loops of the voltage source converter, along with the electrical system has been developed and then linearized around an equilibrium point. This model has been verified against a detailed Simulink model.

The results show a discrepancy between the linear model and the Simulink mode. There are oscillations in the linear model that do not exist in the nonlinear model. The results also show that the discrepancies are not a result of where the linearization point occurs. The eigenvalues of the system do not change much, and the oscillation is similar for different points. The report concludes that further work into the modelling must be done to verify the model such that it can be used to accurately describe the physical system.

Table of Contents

List of Tables

List of Figures

Abbreviations

Abbreviation	Description
AC	Alternating current
BaSS	Electrochemical battery for voltage support in distribution grid
BESS	Battery energy storage system
DC	Direct current
EMC	electromagnetic compatibility
FoL	Forskrift om leveringskvalitet/Regulations on power quality
IGBT	Insulated gate bipolar transistor
LTI	linear time-invariant
MIMO	Multiple-input multiple-output
NTI	Nonlinear time-invariant
PLL	Phase-locked loop
RMS	Root mean square
SISO	Single-input single-output
SOC	State of charge
SOH	State of health
SRF	Synchronous reference frame
VOC	Voltage-oriented control
VSC	Voltage source converter
MOSFET	Metal-oxide- semiconductor field effect transistor

1

Introduction

The increase in distributed energy generation and societies' shift to more electrification has increased the demand for the distribution grid. This increase is attributed to the shift from fossil fuels to renewable energy sources like wind turbines or solar power. This increased demand causes the voltage quality, and sometimes the power quality (explained in section 1.3 in the grid to suffer and necessary measures must be introduced to maintain the voltage quality. Previously the most common method to solve these problems has been grid reinforcements.

1.1 Battery Energy Storage System

An energy storage system is a system that is capable of storing energy to be used at a later time. A BESS utilises a battery as the underlying storage technology. a BESS consists of four main hardware components and software [1] [2].

- Battery Pack
- Power conversion system (PCS)
- Battery management system (BMS)
- Supervisory control system (SCS)

1.1.1 Battery Pack

The battery pack is the actual storage device holding the energy. Individual battery cells are assembled in series and parallel depending on the voltage and current requirements into modules. These modules are assembled into a battery pack capable of supplying sufficient energy and power needed for the application. The battery pack is connected to the PCS.

1.1.2 Power Conversion System

The PCS is a four-quadrant operated alternating current/direct current (AC/DC) converter connecting the battery pack (DC) to the electrical grid (AC). The PCS controls the current flow between the electrical grid and the battery pack. And in result, the active and reactive power. Multiple different types of converters can be utilised, in this thesis, a voltage source converter (VCS) is examined.

1.1.3 Battery Management system

The battery management system monitors the state of the battery pack and individual battery cells. For larger battery systems, multiple BMS may be used to monitor a single module each. They communicate back to the SCS. The BMS monitors the battery cells to maintain safe and optimal operating conditions. It measures the temperature, voltage and current of each cell to ensure it is within the tolerated limits. Based on these measurements the BMS estimates critical conditions of the battery like state of charge (SOC) and state of health (SOH).

1.1.4 Supervisory Control System

The supervisory control system monitors and controls the full system of the battery pack. It controls the energy flow between the battery pack and the electrical grid. The control strategy is dependent on the application requirements of the battery pack.

1.2 BESS in the Distribution Grid

The intermittent energy characteristics of renewable energy sources like photovoltaics (PV) may cause voltage variations throughout the day. Incorporating a BESS into PV systems allows for a more balanced energy flow into the distribution grid [3]. Some use-cases of the BESS can be: Peak load shaving when the demand on the grid is high or power curve smoothing when the PV output is high [4].

1.2.1 Influence on Voltage

The VSC controls the active P and reactive Q power that flows between the BESS and the distribution grid. Assuming that the distribution grid is symmetric, the effect that the active and reactive has on the grid voltage can be simplified to [5]

$$\Delta U = U_1 - U_2 \approx \frac{R_{LN}P + X_{LN}Q}{U_2} \tag{1.1}$$

where R_{LN} and X_{LN} is the line's resistance and reactance. U_2 is the connection point of the battery system and U_1 is the point of common coupling (PCC), assumed stiff (constant) and not affected by the BESS. Figure 1.1 shows a line-diagram of how a battery system can be connected to the grid and its effect on the voltage. From (1.1) it can be seen that

a load in the grid always causes a voltage drop. The influence a BESS has on the grid depend on the active and reactive power that flows into the grid, as well as the total line impedance $Z_{LN} = R_{LN} + j \cdot X_{LN}$.

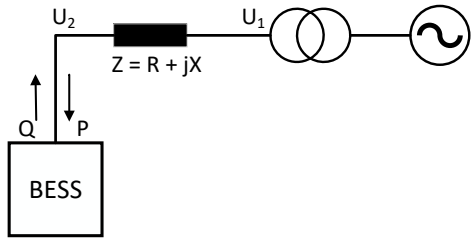

Figure 1.1: One-line diagram of battery effect on grid voltage

Any reactive power is not dependent on the battery capacity or charge, only on the converter. Operating the converter in four-quadrant operation allows the BESS to independently control the reactive and active power flow. In the distribution grid, the $\frac{R}{X}$ is normally high, meaning that it is not enough to control the reactive power flow in and out of the grid to control the voltage, as is usually done in the high voltage transmission grid. The placement of the battery and the line impedance has an effect on how much the BESS is able to influence the voltage. For an optimal control strategy with control of both active and reactive power, the ratio $\frac{R}{X}$ at the battery placement should be known.

1.3 Power Quality

Power quality can be divided into two sections: reliability of supply and voltage quality [6]. FoL [7] defines the power quality parameters and sets limits on the allowed deviation for the voltage problems.

1.3.1 Reliability of Supply

Reliability of supply defines the grid's ability to deliver energy to the end user. It describes both the frequency and duration of voltage interruptions. The interruptions are divided into two classifications

- long-term duration of 3 minutes or more.
- Short-term duration of less than 3 minutes.

1.3.2 Voltage Quality

Voltage quality defines the quality when there is no interruption of delivery. The voltage quality can be reduced in multiple different ways. The voltage qualities that are of interest in this thesis can be divided into these groups and subgroups: [8]

- frequency

- RMS value
  - long-term voltage variations
  - short-term voltage variations
    - rapid voltage changes
    - under voltage (dip)
    - over-voltage (swell)

Long-term Voltage Variations

FoL defines long-term voltage variations as the RMS value of the voltage over a one-minute interval. The quality limits FoL sets are that the voltage value should not exceed $\pm 10\%$ of the nominal voltage, measured over a one-minute interval at the connection point of the distribution grid. For a supply voltage of $230V$ the limit values are $207V < U < 253V$, with U being the RMS value of the voltage at the measured location.

Problems that might arise from long-term voltage variations are faults, disconnections or a breakdown of electrical equipment. This may lead to a shortened life span of the equipment. The most common reasons for long-term voltage variations can be local energy production, changes in the load or a faulty transformer.

Rapid Voltage Changes

FoL defines rapid voltage changes as a change in the RMS voltage inside $\pm 10\%$ of nominal voltage that happens faster than 0.5% of the agreed voltage level per second [7]. Rapid voltage change values are expressed as stationary change and maximal change during a voltage change characteristic. Which is defined by FoL as the change in the voltage RMS value evaluated per half period as a function of time, between periods where the voltage has been stable for a minimum of a second. The voltage is considered stable when it is between $\pm 0.5\%$ of the agreed supply voltage.

$$\%U_{stationary} = \frac{\Delta U_{stationary}}{U_{agreed}} \cdot 100\% \tag{1.2}$$

$$\%U_{max} = \frac{\Delta U_{max}}{U_{agreed}} \cdot 100\% \tag{1.3}$$

Where $U_{stationary}$ is the stationary voltage change during the voltage change characteristic, ΔU_{max} is the maximal voltage difference during the voltage change characteristic and U_{agreed} is the agreed voltage supply voltage. Table **??** shows how many violations are allowed within a 24-hour time period.

Short-term over voltage, short-term under voltage and rapid voltage changes	Maximum number allowed within 24 hour period
	$0.23kV \leq U_N \leq 35kV$
$\%U_{stationary} \geq 3\%$	24
$\%U_{max \geq 5\%}$	24

Table 1.1: Maximum allowed voltage violations within a 24-hour time period.

Short-term under voltage(dip)

FoL defines dip as a fast reduction in the RMS voltage to under 90% of the nominal voltage (or agreed supply voltage), but greater than 5%, with a period between ten milliseconds to one minute[7]. The maximum allowed deviations are the same as for rapid voltage changes and can be found in Table **??**. Voltage dip is together with disconnections the power quality problem that inflicts the most economical losses [6]. The most common causes of dips are short circuits in the grid, reconnection of faults and large load changes. It can cause failure or disconnections of electrical equipment.

Short-term over voltage(swell)

FoL defines swell as a fast increase in the RMS voltage to over 110% of the nominal voltage (or agreed supply voltage), with a period between ten milliseconds to one minute. The maximum allowed deviations are the same as for rapid voltage changes and can be found in Table **??**. A common cause of swells can be a sudden disconnection of large loads. Swells are less common than dips, and in Norway, they are ten times less likely to occur [6].

1.4 BaSS Project

The BaSS project (batteri som spenningsstøtte or electrochemical battery for voltage support in distribution grid) is a research project at SINTEF Energy. It is researching how to facilitate that battery energy storage systems (BESS) can become an alternative to grid reinforcements, and when this is the most socio-economic solution [8].

BaSS has different work packages that aim to research different topics for a BESS [9]

- **BESS as a grid service:** Research into when a BESS can contribute with voltage support and when it has limited value.
- **Operation strategies and communication needs for operating a BESS:** Control and operation strategies for a BESS including simulation.
- **Testing BESS as voltage support:** Testing out operation strategies in both a Smartgrid-lab and on real distribution grids.

- **Developing a methodology for assessment and specification of BESS as voltage support:** Develop methodologies for evaluating a BESS against traditional grid reinforcement.

This project is under the second work package as modelling is an integral part of developing control strategies for a system.

1.5 Motivation and Scope

The goal of this project thesis is to create a small-signal linearized model of the voltage source converter and the electrical grid it is connected to. This model is to be verified that it properly describes the dynamic system that is linearized. When the linearized model has been properly verified, it is to be utilized in a master's thesis to develop a control algorithm for voltage support in the distribution grid. This project does not go into any control strategies, it is solely a description of the modelling and linearization of the VSC model.

2

Method

2.1 State-Space Model

A state-space model is a system that relates state variables and input variables together with a first-order differential equation. The equations can be nonlinear or linear. A state-space model is used to accurately describe the physical system that we wish to control.

2.1.1 Nonlinear Time-invariant System

Most systems that accurately describe the physical world are non-linear and time-variant. [10] These can be written on the form

$$\begin{aligned} \dot{\boldsymbol{x}}(t) &= \boldsymbol{f}(\boldsymbol{x}(t), \boldsymbol{u}(t), t) \\ \boldsymbol{y}(t) &= \boldsymbol{g}(\boldsymbol{x}(t), \boldsymbol{u}(t), t) \end{aligned} \tag{2.1}$$

where $\boldsymbol{f}$ and $\boldsymbol{g}$ are nonlinear functions. The system in this project is a nonlinear time-invariant (NTI) system. By using the dq-transformation explained in section 2.4, the time-varying system can be transformed into a NTI system under steady-state conditions. [11] The NTI system is expressed on the form

$$\begin{aligned} \dot{\boldsymbol{x}} &= f(\boldsymbol{x}, \boldsymbol{u}) \\ \boldsymbol{y} &= g(\boldsymbol{x}, \boldsymbol{u}) \\ \boldsymbol{x} &= \begin{bmatrix} x_1 & x_2 & \dots & x_n \end{bmatrix}^T \\ \boldsymbol{u} &= \begin{bmatrix} u_1 & u_2 & \dots & u_n \end{bmatrix}^T \\ \boldsymbol{y} &= \begin{bmatrix} y_1 & y_2 & \dots & y_n \end{bmatrix}^T \end{aligned} \tag{2.2}$$

where $\boldsymbol{f}$ and $\boldsymbol{g}$ are the same nonlinear functions as above, $\boldsymbol{x}$ is a vector of the state space variables, $\boldsymbol{u}$ is a vector of the state space inputs and $\boldsymbol{y}$ is the output vector of the system.

2.1.2 Linear Time-invariant System

For some nonlinear systems, it is possible to approximate linear equations that accurately describe the system under certain conditions. A linearized model is easier to analyze when it comes to stability, and control strategies that are dependent on a linear model can be utilized. With the input signals $\boldsymbol{u}_0$ and state variables $\boldsymbol{x}_0$, the equilibrium point for the nonlinear system can be expressed as

$$f(\boldsymbol{x}_0, \boldsymbol{u}_0) = \dot{\boldsymbol{x}}_0 = 0 \tag{2.3}$$

This is a steady-state point of the system, and (2.3) can be solved for the steady state variables $\boldsymbol{x}_0$ as a function of the input signals $\boldsymbol{u}_0$. For some small perturbation $\Delta\boldsymbol{u}$ in the input signal, there is only a small perturbation $\Delta\boldsymbol{x}$ in the state variables. Expressing the input signals and state variables with small perturbations as

$$\begin{aligned} \boldsymbol{x} &= \boldsymbol{x_0} + \Delta\boldsymbol{x} \\ \boldsymbol{u} &= \boldsymbol{u_0} + \Delta\boldsymbol{u} \end{aligned} \tag{2.4}$$

the system can be linearized using the first order Taylor-series of the nonlinear equations (2.2) and a linear time-invariant (LTI) state space model is expressed on the form

$$\begin{aligned} \Delta\dot{\boldsymbol{x}} &= \boldsymbol{A}\Delta\boldsymbol{x} + \boldsymbol{B}\Delta\boldsymbol{u} \\ \Delta\dot{\boldsymbol{y}} &= \boldsymbol{C}\Delta\boldsymbol{x} + \boldsymbol{D}\Delta\boldsymbol{u} \end{aligned} \tag{2.5}$$

where the system matrices $\boldsymbol{A}$, $\boldsymbol{B}$, $\boldsymbol{C}$ and $\boldsymbol{D}$ are found using the jacobian of the nonlinear functions. (2.2). This is the small-signal model of the system, where the system matrices are

$$\begin{aligned} \boldsymbol{A} &= \frac{\partial f(\boldsymbol{x}, \boldsymbol{u})}{\partial \boldsymbol{x}}\Big|_{\substack{\boldsymbol{x}=\boldsymbol{x}_0 \\ \boldsymbol{u}=\boldsymbol{u}_0}}, \quad \boldsymbol{B} = \frac{\partial f(\boldsymbol{x}, \boldsymbol{u})}{\partial \boldsymbol{u}}\Big|_{\substack{\boldsymbol{x}=\boldsymbol{x}_0 \\ \boldsymbol{u}=\boldsymbol{u}_0}} \\ \boldsymbol{C} &= \frac{\partial g(\boldsymbol{x}, \boldsymbol{u})}{\partial \boldsymbol{x}}\Big|_{\substack{\boldsymbol{x}=\boldsymbol{x}_0 \\ \boldsymbol{u}=\boldsymbol{u}_0}}, \quad \boldsymbol{D} = \frac{\partial g(\boldsymbol{x}, \boldsymbol{u})}{\partial \boldsymbol{u}}\Big|_{\substack{\boldsymbol{x}=\boldsymbol{x}_0 \\ \boldsymbol{u}=\boldsymbol{u}_0}} \end{aligned} \tag{2.6}$$

2.1.3 Transfer Function Representation

For a lumped LTI system, expressed as a set of equations on the form

$$\begin{aligned} \dot{\boldsymbol{x}}(t) &= \boldsymbol{A}\boldsymbol{x}(t) + \boldsymbol{B}\boldsymbol{u}(t) \\ \dot{\boldsymbol{y}}(t) &= \boldsymbol{C}\boldsymbol{x}(t) + \boldsymbol{D}\boldsymbol{u}(t) \end{aligned} \tag{2.7}$$

the transfer function matrix $\boldsymbol{G}(s)$ can be calculated by applying the Laplace transform on (2.7). [10] $\boldsymbol{G}$ can be expressed as

$$\boldsymbol{G}(s) = \frac{\boldsymbol{y}(s)}{\boldsymbol{u}(s)} = \boldsymbol{C}\left(s\boldsymbol{I} - \boldsymbol{A}\right)^{-1}\boldsymbol{B} + \boldsymbol{D} \tag{2.8}$$

The transfer function matrix is unique and contains every combination of input-to-output functions. $\boldsymbol{G}$ makes it possible to extract the SISO transfer functions from each input $\boldsymbol{u}$ to each output $\boldsymbol{y}$.

The converse problem, to find a state space representation on the form (2.7) from the transfer function matrix (2.8) can also be done. This is called *realization*. If a realization is possible to implement, there are infinitely many representations making the problem complex. The realization of the transfer matrix is not discussed more in this project as the state space representation is derived using the physical model of the converter.

2.2 Stability analysis

The small-signal dynamics of the LTI-system can be analyzed using the eigenvalues λ of the A-matrix. The location in the complex plane of the eigenvalues determines some of the dynamics of the system. The eigenvalues λ are defined as the non-trivial solution to the equation[12]

$$\boldsymbol{A}\boldsymbol{\Phi}_i = \lambda_i \boldsymbol{\Phi}_i \tag{2.9}$$

where $\boldsymbol{\Phi}$ is the *right eigenvector* of $\boldsymbol{A}$. The non-trivial solutions can be found by solving the characteristic equation

$$det\left(\boldsymbol{A} - \lambda\boldsymbol{I}\right) = 0 \tag{2.10}$$

The eigenvalues of the system may be real or a complex conjugate pair written on the form

$$\lambda_i = \alpha + j\omega \tag{2.11}$$

By defining the *left eigenvector* $\boldsymbol{\Psi}$ which satisfies

$$\boldsymbol{\Psi}_i\boldsymbol{A} = \lambda_i \boldsymbol{\Psi}_i \tag{2.12}$$

and normalizing the vectors such that

$$\boldsymbol{\Psi}_i\boldsymbol{\Phi}_i = 1 \tag{2.13}$$

it is possible to define a system $\Delta\dot{\boldsymbol{x}}$, together with a decoupled system with the diagonal matrix $\boldsymbol{\Lambda}$, where the diagonal are the eigenvalues λ_i. of the original system. The original system and the new decoupled system are described as

$$\Delta\dot{\boldsymbol{x}} = \boldsymbol{A}\Delta\boldsymbol{x} \tag{2.14}$$

$$\Delta \dot{\boldsymbol{x}} = \boldsymbol{\Phi} \boldsymbol{z} \tag{2.15}$$

$$\dot{\boldsymbol{z}} = \boldsymbol{\Lambda} \boldsymbol{z} \tag{2.16}$$

The dynamics of the decoupled system $\boldsymbol{z}$ can easily be found by solving the differential equations, and because $\boldsymbol{\Lambda}$ is a diagonal matrix, each time response will only be dependent on its eigenvalue. The solution of the decoupled system is

$$z_i(t) = z_i(0) e^{\lambda_i t} \tag{2.17}$$

The time response of the decoupled system can be found for real and complex eigenvalues. A positive real eigenvalue leads to an exponential increase, while a negative real eigenvalue leads to an exponential decay in the response. The complex part contributes to a sinusoidal response. This means that for an asymptotic stable response, the real part of the eigenvalue must have a negative part. The time response for the original state variable $\boldsymbol{x}_i$ can be found from

$$\Delta \boldsymbol{x}(t) = \sum_{i=1}^{n} \boldsymbol{\Phi}_i \boldsymbol{\Psi}_i \Delta \boldsymbol{x}(0) e^{\lambda_i t} \tag{2.18}$$

It can be seen that the time response of the original system $\Delta \boldsymbol{x}$ is given by a linear combination of the decoupled time responses. And the stability of the small-signal model can be determined based on the decoupled system.

2.3 Per-unit system

For electrical systems, different systems operate on varied amount of voltage levels and frequencies. This makes it cumbersome to compare systems with each other. Instead of representing parameters with their actual value, a per-unit system is introduced. The values are expressed as a fraction of base quantities. The per unit (pu) value is defined as [13]

$$\text{pu quantity} = \frac{\text{actual quantity}}{\text{base value of quantity}} \tag{2.19}$$

The necessary base values of the system are: Apparent power S_b, voltage V_b, current I_b, impedance Z_b, and angular velocity ω_b. For a three-phase system, S_b is chosen as the rated apparent power, V_b is chosen as the peak nominal voltage and ω_b is chosen as the grid's angular velocity. I_b and Z_b are chosen as

$$I_b = \frac{2}{3} \frac{S_b}{V_b} \tag{2.20}$$

$$Z_b = \frac{V_b}{I_b} \tag{2.21}$$

It is also useful to define a resistance base R_b and the inductance base L_b as

$$Z_b = R_b = \omega_b L_b \tag{2.22}$$

2.4 Two-Phase Representation in Synchronous Reference Frame

A three-phase electrical system consisting of three voltages and three currents. For a balanced three-phase system where the phase shift between the phases is $120°$, it is possible to represent these in an equivalent two-phase system in space vector form.[14] For an unbalanced system it would be necessary to also represent a zero-sequence component. This component is disregarded in this project. The transformation into a two-phase representation is done via Clarke and Park transformation explained below.

2.4.1 Clarke transformation

The three-phase system is represented in a two-phase system on the $\alpha\beta$ plane. This is seen as a complex plane with α and β on the real and imaginary axis. The space vector notation is represented as $\boldsymbol{x}^{\alpha\beta} = x^{\alpha} + j \cdot x^{\beta}$. The space vector $\boldsymbol{x}^{\alpha\beta}$ is said to be in stationary reference coordinates. This means that the $\alpha\beta$ space vector has the same frequency as the original three-phase system in abc. The transformation from a three-phase system can be expressed in matrix form as

$$\begin{bmatrix} x^{\alpha} \\ x^{\beta} \end{bmatrix} = \frac{2}{3} \begin{bmatrix} 1 & -\frac{1}{2} & -\frac{1}{2} \\ 0 & \frac{\sqrt{3}}{2} & -\frac{\sqrt{3}}{2} \end{bmatrix} \begin{bmatrix} x^{a} \\ x^{b} \\ x^{c} \end{bmatrix} \tag{2.23}$$

The constant $\frac{2}{3}$ is used for scaling the space vector to the same amplitude as the phase variable. The $\boldsymbol{v}^{\alpha\beta}$ representation rotates at the same sinusoidal frequency as the three-phase system. This implies that if we want to control any of these signals we need to track and control a sinusoidal signal. A PI-controller is not able to ensure zero steady-state error, and because PI-controllers are to be used as explained in section 3.4 and section 3.3 this is not optimal. The Park transformation is introduced below which solves this.

2.4.2 Park Transformation

Because the Clarke representation is in a stationary reference frame that rotates at some angular frequency it is possible to represent the space vector in a rotating reference frame. This reference frame can be expressed as

$$\boldsymbol{x}^{dq} = \boldsymbol{x}^{\alpha\beta} e^{-j \cdot \theta} \tag{2.24}$$

The equivalent matrix form is

$$\begin{bmatrix} x^{d} \\ x^{q} \end{bmatrix} = \begin{bmatrix} \cos\theta & \sin\theta \\ -\sin\theta & \cos\theta \end{bmatrix} \begin{bmatrix} x^{\alpha} \\ x^{\beta} \end{bmatrix} \tag{2.25}$$

This transformation is called Park or dq transformation, and it transforms the space vector into a synchronously rotating reference frame. The dq transformation can be seen as an

observation of the $\alpha\beta$ space vector into a space vector that rotates with the fundamental frequency $\theta = \omega t$. The dq space vector $x^{dq} = x^d + j \cdot x^q$. The dq frame is in a complex plane with dc quantities in a steady state. This is useful for analysis, as well as control algorithms like a PI-controller, as there is zero steady-state error.

2.5 Power calculations

The Clarke and Park transform is advantageous when performing power calculations. It can be seen that in a synchronous reference frame the apparent power s can be expressed as

$$s = p + j \cdot q = \boldsymbol{v}^{dq} \cdot \bar{\boldsymbol{i}}^{dq} = v^d i^d + v^q i^q + j \left(-v^d i^q + v^q i^d\right) \tag{2.26}$$

and it can be seen that the active p and reactive q power are

$$p = v^d i^d + v^q i^q \tag{2.27}$$

$$q = -v^d i^q + v^q i^d \tag{2.28}$$

By using a voltage-oriented synchronous reference frame oriented in the d-axis, it is possible to obtain independent control of the active and reactive power. The apparent power when $v^q = 0$ becomes

$$s = v^d i^d - j \left(v^d i^q)\right) \tag{2.29}$$

Having independent control of the active power from i^d and reactive power from i^q allows us to better achieve the control objectives and implement control strategies. The necessary grid synchronization is explained in section 3.4.

3

Overview of Voltage Source Converter

3.1 Voltage Source Converter

A two-level converter is the most commonly used voltage source converter (VSC) for applications up to dc-side voltages up to approximately 1800V [14]. It is used in drive systems for cars, industrial drives and low-voltage grid-connected converters. The topology and function of the two-level VSC shown in Figure 3.2 are explained below. The complete overview of the control system for the VSC can be seen in Figure 3.1.

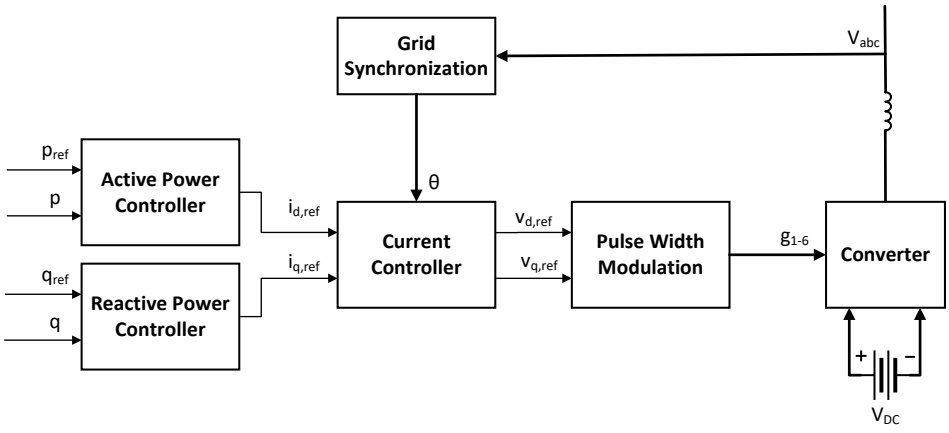

Figure 3.1: Overview of control system for VSC

Two capacitors are connected in series across the DC input (in this case a battery). The capacitors act as short-term energy storage, and it is assumed that the capacitors are sufficiently large such that the voltage stays constant. Three phase legs are connected in parallel to the capacitors, with two controllable switches connected in series. These switches can be either an insulated gate bipolar transistor (IGBT) or a metal-oxide-semiconductor field effect transistor (MOSFET). One anti-parallel diode is connected to each controllable switch [15]. The output on the AC side is connected to the midpoint of each phase leg. The voltage on the phase leg only depends on the DC side voltage and the status of the switches controlling that phase leg.

3.2 Pulse Width Modulator

The Pulse width modulator (PWM) is the connection between the control system and the physical converter. The PWM controls the controllable switches in the VSC. To be able to control both the amplitude and the frequency of the output voltage, different control strategies can be used. A common method is to use a sinusoidal control signal v_{contrl} at the desired frequency that is compared to a triangular carrier signal v_{tri} [15]. The switches will turn on and off depending on the state of these two signals. Every pair of gates are controlled by one sinusoidal reference signal and a carrier signal. For full utilization of the DC voltage, it is possible to use a strategy called third harmonic injection, this allows for a higher output voltage. For modelling purposes, the carrier method, with a switching period of T_{sw} is assumed.

The PWM time delay can be approximated by a first order time delay transfer function dependent on the switching period.

$$h_c(s) \approx \frac{1}{1 + \frac{T_{sw}}{2} \cdot s} = \frac{1}{1 + T_{sum,c} \cdot s} \tag{3.1}$$

The modulation index relates the amplitude of the alternating voltage component to dc-side voltage [14], and choosing a base value for the DC voltage as $V_{b,dc} = 2V_b$. It is assumed that the output voltage of the converter $\boldsymbol{v}_{cv}^{dq}$ is equal to the voltage reference value $\boldsymbol{v}_{cv}^{*,dq}$. The modulation index is then defined as

$$\boldsymbol{m}^{dq} = \frac{2V_{cv}}{V_{dc}} = \frac{\boldsymbol{v}_{cv}^{dq}}{v_{dc}} \approx \frac{\boldsymbol{v}_{cv}^{*,dq}}{v_{dc}} \tag{3.2}$$

The output voltage of the converter can then be approximated as

$$\boldsymbol{v}_{cv}^{dq} \approx \boldsymbol{m}^{dq} \cdot v_{dc} \frac{1}{1 + T_{sum,c} \cdot s} \approx \boldsymbol{v}_{cv}^{*,dq} \cdot \frac{1}{1 + T_{sum,c} \cdot s} \tag{3.3}$$

The nonlinearity introduced by the DC-voltage is removed by using the pu value of the voltage reference as the modulation index for the PWM-signal. Figure 4.2 shows how

this is implemented in the controller by dividing the reference voltage signal with the DC-voltage.

3.3 Current Controllers

The current controllers are implemented in the dq frame rotating with the angular speed $\omega_g = 2\pi f_g$, with f_g being the grid frequency [16]. The goal of the controller is to have independent control of i^d and i^q to control the active and reactive power as explained in section 2.5. This is done by using voltage-oriented control (VOC). Obtaining this can be done by manipulating the voltage balance equation (4.5). This can be rewritten into

$$\boldsymbol{v}_{cv}^{dq} = \boldsymbol{v}_{o}^{dq} + r_f \boldsymbol{i}_{cv}^{dq} + \frac{l_f}{r_f}\frac{d}{dt}\boldsymbol{i}_{cv}^{dq} + j \cdot \omega_g l_f \boldsymbol{i}_{cv}^{dq} \tag{3.4}$$

These can be re-written into their respective d and q components

$$v_{cv}^{d} = v_{o}^{d} + r_f i_{cv}^{d} + \frac{l_f}{\omega_b}\frac{d}{dt} i_{cv}^{d} - \omega_g l_f i_{cv}^{q} \tag{3.5}$$

$$v_{cv}^{q} = v_{o}^{q} + r_f i_{cv}^{q} + \frac{l_f}{\omega_b}\frac{d}{dt} i_{cv}^{q} + \omega_g l_f i_{cv}^{d} \tag{3.6}$$

It can be seen from (3.5) and (3.6) that the output current i_{cv}^{dq} is controlled by the converter voltage v_{cv}^{dq}. The controller is chosen as a PI-controller with a voltage feedforward term and decoupling terms for the dq-axis. The controllers are

$$v_{PI}^{d} + v_{o}^{d} - \omega_g l_f i_{cv}^{q} = v_{o}^{d} + r_f i_{cv}^{d} + \frac{l_f}{\omega_b}\frac{d}{dt} i_{cv}^{d} - \omega_g l_f i_{cv}^{q} \tag{3.7}$$

$$v_{PI}^{q} + v_{o}^{q} + \omega_g l_f i_{cv}^{d} = v_{o}^{q} + r_f i_{cv}^{q} + \frac{l_f}{\omega_b}\frac{d}{dt} i_{cv}^{q} + \omega_g l_f i_{cv}^{d} \tag{3.8}$$

The implementation of the decoupled controllers is shown in Figure 4.2. From (3.7) and (3.8), the transfer functions for the converter currents are

$$h_{cv}^{dq}(s) = \frac{v_{cv}^{dq}(s)}{i_{cv}^{dq}(s)} = \frac{1}{r_f + \frac{l_f}{\omega_b} \cdot s} = \frac{1}{r_f} \cdot \frac{1}{1 + T_{cv} \cdot s} \tag{3.9}$$

The multiple-input multiple-output (MIMO) system has been reduced to two equal single-input single-output (SISO) systems. Using this transfer function together with the transfer function obtained for the converter (3.1). A PI-controller is implemented. The resulting transfer function for the complete inner loop current controller is

$$h_{ol,cc}^{dq}(s) = k_{pc}\frac{1+T_{ic}\cdot s}{T_{ic}\cdot s}\frac{1}{1+T_{sum,c}\cdot s}\cdot\frac{1}{r_f}\cdot\frac{1}{1+T_{cv}\cdot s} \tag{3.10}$$

The inner loop current controllers are tuned using pole cancellation by modulus optimum. The proportional gain is tuned to achieve critical damping of the closed loop function. The PI-controller parameters are

$$T_{i,c} = T_{c,v} \tag{3.11}$$

$$k_{p,c} = \frac{T_{cv}\cdot r_f}{2\cdot T_{sum,c}} \tag{3.12}$$

3.4 Grid Synchronization

Grid synchronization must be done to achieve independent control of active and reactive power as shown in section 2.5. The method for grid synchronization that will be used is a Phase-Locked Loop (PLL) system. The PLL is a closed-loop system that outputs the angle θ used in the dq-transformation. Figure 4.4 shows the feedback loop of the PLL. It works on the concept that $v_q = 0$ when the SRF is synchronized with the grid voltage. The estimated v_d and v_q values are filtered through a first-order low-pass filter and sent through an inverse tangent function to estimate the phase angle error [17].

The PLL is a nonlinear closed-loop system because of the dq-transform. It is possible to linearize the system using a small-signal model. Assuming small deviations from the grid orientation the nonlinear parts are linearized around this. This is a valid assumption during normal operation [14].

$$\sin\Delta\theta \approx \Delta\theta \tag{3.13}$$

$$\cos\Delta\theta \approx 1 \tag{3.14}$$

The PI-controller for the PLL is designed using the small signal model of the PLL. The open loop model of the current controller is modelled as the transfer function

$$h_{ol,pll}(s) = k_{p,pll}\frac{1+T_{i,pll}\cdot s}{T_{i,pll}\cdot s}\cdot\frac{2\pi}{s}\cdot\frac{1}{1+T_{f,pll}\cdot s} \tag{3.15}$$

The PLL controller is tuned using symmetrical optimum. This is a standard method of tuning transfer functions containing two integrators [16]. The idea is to choose the crossover frequency of the transfer function as the geometric mean of the two corner frequencies. this is done to obtain the maximum phase margin ψ. The PI-controller parameters are chosen as

$$T_{i,pll} = \alpha^2\cdot T_{f,pll} \tag{3.16}$$

$$k_{p,pll} = \frac{1}{\alpha \cdot 2\pi \cdot T_{f,pll}} \tag{3.17}$$

Where α is a free tuning-variable that can be chosen depending on the phase margin requirements.

3.5 Outer Control Loops

The outer control loops control the reference value $\boldsymbol{i}^{*,dq}$ that is used for the current controllers in section 3.3. Depending on the control objective, different types of outer control loops can be implemented. The relevant control objectives for voltage support in the distribution grid are

- Control of active power flow on AC-side
- Control of reactive power flow on AC-side
- Control of AC-side voltage

As shown in subsection 1.2.1 the line resistance and reactance ratio $\frac{R}{X}$ in the grid determines the optimal control strategy for the outer loop controllers. The modelling of the outer loop controllers is not within the scope of this thesis, and is not looked further into.

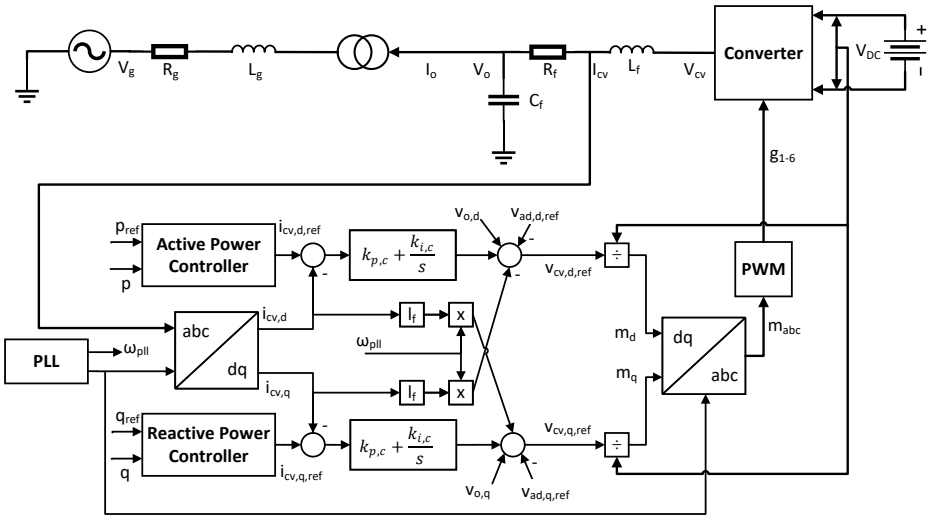

Figure 3.2: Detailed overview of control system for VSC

4

Modelling of Voltage Source Converter

In chapter 3 the complete model of a VSC is explained. In this chapter, an NTI model of the VSC is developed, which can be linearized into an LTI system. As the focus of this project is the inner loop of the VSC, the two outer loop controllers from section 3.5 have not been developed. Figure 4.1 shows which parts of the VSC that is being modelled, including the electrical system. The outer control loops for the active power and reactive power are not found. The method used for finding the non-linear equations is based on the approach in [18][17].

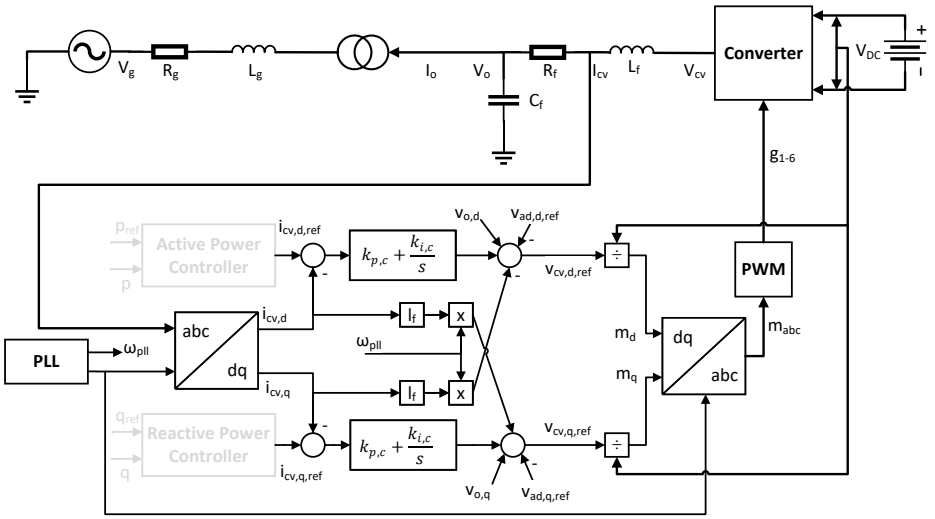

Figure 4.1: Model of VSC that model is developed after

4.1 Modelling conventions

The naming convention for the model is that upper-case letters are physical values, while lower-case letters are in per-unit. Superscripts describe which reference frame the parameter is in, while subscripts describe what signal it is. Space vectors are bolded, and represented as in subsection 2.4.1. An explanation of subscripts and superscripts can be found in Appendix A.

4.2 Electrical system

Using voltage balance, three differential equations can be derived in the dq-reference frame describing the electrical system for the AC-side in Figure 4.1. L_f, C_f and R_f describe the filter components of the converter, while L_g and R_g are the grid's inductance and resistance. In the α/β frame the equations are

$$\boldsymbol{V}_{cv}^{\alpha\beta} = \boldsymbol{V}_{f}^{\alpha\beta} + R_f \boldsymbol{I}_{cv}^{\alpha\beta} + L_f \frac{d}{dt} \boldsymbol{I}_{cv}^{\alpha\beta} \tag{4.1}$$

$$C_f \frac{d}{dt} \boldsymbol{V}_{o}^{\alpha\beta} = \boldsymbol{I}_{cv}^{\alpha\beta} - \boldsymbol{I}_{o}^{\alpha\beta} \tag{4.2}$$

$$\boldsymbol{V}_{g}^{\alpha\beta} = R_g \boldsymbol{I}_{g}^{\alpha\beta} + L_g \frac{d}{dt} \boldsymbol{I}_{g}^{\alpha\beta} + \boldsymbol{V}_{f}^{\alpha\beta} \tag{4.3}$$

By converting the equations into per-unit and transforming them into the dq-frame. the nonlinear equations for the system become

$$\frac{d}{dt}\boldsymbol{v}_o^{dq} = \frac{\omega_b}{c_f}\boldsymbol{i}_{cv}^{dq} - \frac{\omega_b}{c_f}\boldsymbol{i}_o^{dq} - j \cdot \omega_g \omega_b \boldsymbol{v}_o^{dq} \tag{4.4}$$

$$\frac{d}{dt}\boldsymbol{i}_{cv}^{dq} = \frac{\omega_b}{l_f}\boldsymbol{v}_{cv}^{dq} - \frac{\omega_b}{l_f}\boldsymbol{v}_o^{dq} - \left(\frac{r_f \omega_b}{l_f} + j \cdot \omega_g \omega_b\right)\boldsymbol{i}_{cv}^{dq} \tag{4.5}$$

$$\frac{d}{dt}\boldsymbol{i}_o^{dq} = \frac{\omega_b}{l_g}\boldsymbol{v}_o^{dq} - \frac{\omega_b}{l_g}\boldsymbol{v}_g^{dq} - \left(\frac{r_g \omega_b}{l_g} + j \cdot \omega_g \omega_b\right)\boldsymbol{i}_o^{dq} \tag{4.6}$$

4.3 Inner Loop Current Controllers

The inner loop current controllers are controlled by PI-controllers as described in section 3.3. The voltage reference $\boldsymbol{v}_{cv}^{*,dq}$, expressed as (4.7) is the output of the decoupled current controllers with a feedforward term for the active damping and the voltage at the connection to the grid. The integrator states of the current controllers are expressed as (4.8).

$$\boldsymbol{v}_{cv}^{*,dq} = k_{p,c}\left(\boldsymbol{i}_{cv}^{*,dq} - \boldsymbol{i}_{cv}^{dq}\right) + k_{i,c}\boldsymbol{\gamma}^{dq} + j \cdot l_f \omega_{pll}\boldsymbol{i}_{cv}^{dq} + \boldsymbol{v}_o^{dq} - \boldsymbol{v}_{ad}^{*,dq} \tag{4.7}$$

$$\frac{d}{dt}\boldsymbol{\gamma}^{dq} = \boldsymbol{i}_{cv}^{*,dq} - \boldsymbol{i}_{cv}^{dq} \tag{4.8}$$

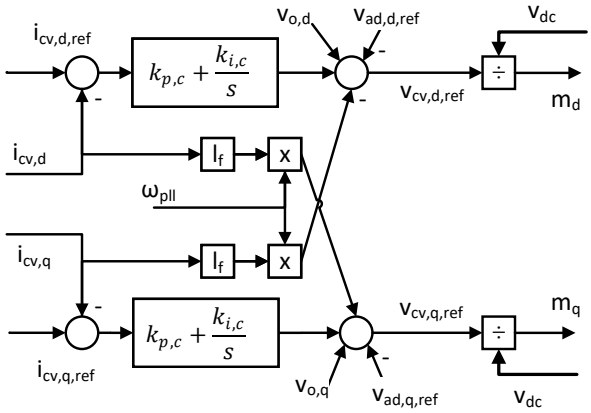

Figure 4.2: Decoupled inner loop current controller

4.4 Active Damping

Active damping of the output voltage of the current controllers is implemented. This is done to cancel out oscillations in the LC filter of the VSC. Figure 4.3 shows how the filter is implemented in this case. by using a low-pass first order filter to isolate high-frequency oscillations in the reference voltage. This is then subtracted from the voltage reference going to the gate signal. The state φ^{dq} for the filter is given by (4.9) and output of the filter that is fed back into the reference voltage is given by (4.10).

$$\frac{d}{dt}\boldsymbol{\varphi}^{dq} = \omega_{ad}\left(\boldsymbol{v}_o^{dq} - \boldsymbol{\varphi}^{dq}\right) \tag{4.9}$$

$$\boldsymbol{v}_{ad}^{*,dq} = k_{ad}\left(\boldsymbol{v}_o^{dq} - \boldsymbol{\varphi}^{dq}\right) \tag{4.10}$$

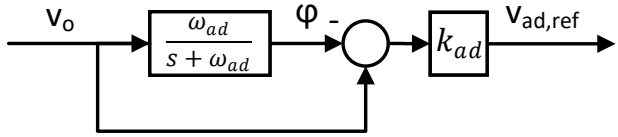

Figure 4.3: Active damping of voltage reference

4.5 Phase Locked Loop

The phase locked loop described in section 3.4 is implemented as shown in Figure 4.4. The filtered voltage state $\boldsymbol{v}_{pll}^{dq}$ for the PLL is given as (4.11). An inverse tangent function is used on the low-pass filtered voltage measurements, giving the integrator state ε_{pll} for the PI-controller as given by (4.12). The phase angle difference $\delta\theta_{pll}$ between the PLL and grid voltage is given by (4.13). The algebraic equations (4.14), (4.15) and (4.16) are the output of the PI, the angular frequency of the PLL and the grid voltage as a function of the PLL.

$$\frac{d}{dt}\boldsymbol{v}_{pll}^{dq} = \omega_{lp,pll}\left(\boldsymbol{v}_o^{dq} - \boldsymbol{v}_{pll}^{dq}\right) \tag{4.11}$$

$$\frac{d}{dt}\varepsilon_{pll} = \arctan\left(\frac{v_{pll,q}}{v_{pll,d}}\right) \tag{4.12}$$

$$\frac{d}{dt}\delta\theta_{pll} = \delta\omega_{pll}\omega_b \tag{4.13}$$

$$\delta\omega_{pll} = k_{p,pll}\cdot\arctan\left(\frac{v_{pll}^q}{v_{pll}^d}\right) + k_{i,pll}\cdot\epsilon_{pll} \tag{4.14}$$

$$\omega_{pll} = \delta\omega_{pll} + \omega_g \tag{4.15}$$

$$\boldsymbol{v}_g^{dq} = \hat{v}_g e^{-j\delta\theta_{pll}} = \hat{v}_g \cdot (\cos(\delta\theta_{pll}) - j \cdot \sin(\delta\theta_{pll})) \tag{4.16}$$

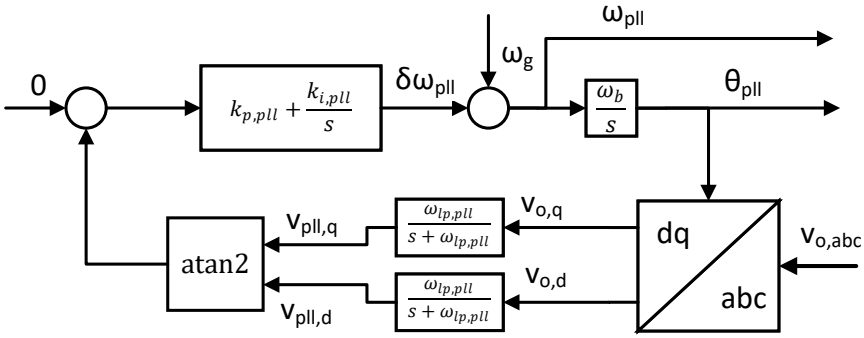

Figure 4.4: Phase Locked Loop diagram

4.6 Nonlinear State Space Model

The complete model of all differential equations on the d and q-axis can be found in appendix B. The linear state space model that is used for further work is calculated using this NTI system. As explained in subsection 2.1.1 this system is time-invariant due to dq-transformation.

4.7 Linear State Space Model

The LTI system is derived using the methods explained in subsection 2.1.2. The complete linear state space model can be found in appendix C. The system has the state variable vector $\boldsymbol{x}$ and input signal vector $\boldsymbol{u}$.

$$\begin{aligned} \boldsymbol{x} &= \begin{bmatrix} v_o^d & v_o^q & i_{cv}^d & i_{cv}^q & \gamma^d & \gamma^q & i_o^d & i_o^q & \varphi^d & \varphi^q & v_{pll}^d & v_{pll}^q & \epsilon_{pll} & \delta\theta_{pll} \end{bmatrix} \\ \boldsymbol{u} &= \begin{bmatrix} i_{cv}^{*,d} & i_{cv}^{*,q} & \hat{v}_g & \omega_g \end{bmatrix} \end{aligned} \tag{4.17}$$

5

Simulation Results

5.1 Verification of linearized model

A detailed Simulink model of the VSC with decoupled current controllers, feedforward and PLL has been developed at SINTEF. The linearized model is compared with this to verify the accuracy of the linearized model.

The NTI system is linearized around $i_{cv}^{*,d} = 0.5$ to compare it to the detailed model. Figure 5.1 shows the comparison of the two models. A step response from 0.5 pu to 0.6 pu in the reference current is tested. The figure shows that there are oscillations in the linear model that are not present in the detailed Simulink model. This is the case both around the linearized point $i_{cv}^{*,d} = 0.5$ and for the higher value in the step response. Figure 5.2 compares the two models during the transient stage of the step response. The Simulink model has some overshoot, but settles down quickly, while the linearized model has less overshoot, but starts oscillating as shown in Figure 5.1. The same response is found when the step response goes back to the linearized point. The cause of the oscillations of the system can be found in the eigenvalues seen in Figure 5.5, where all the eigenvalues are on the negative real part of the plane, with complex conjugate parts. It can be seen that the rise time of the two models is the same, and the sudden change of value during the transient period occurs for both models, at slightly different amplitudes.

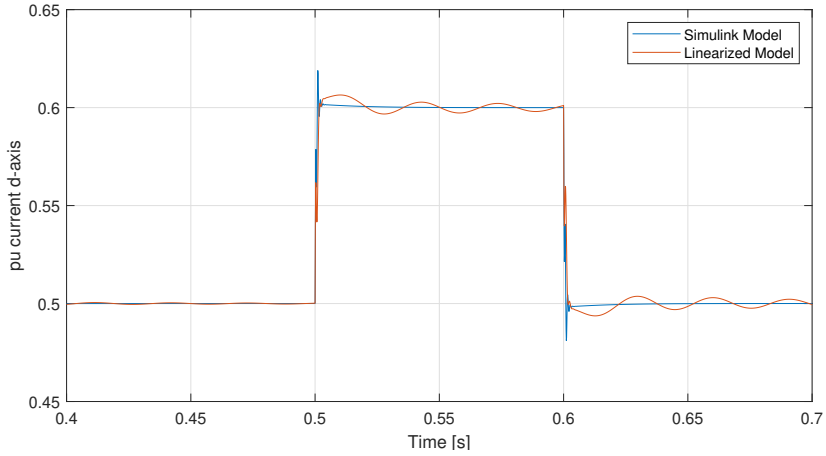

Figure 5.1: Comparison of detailed Simulink model and linearized model

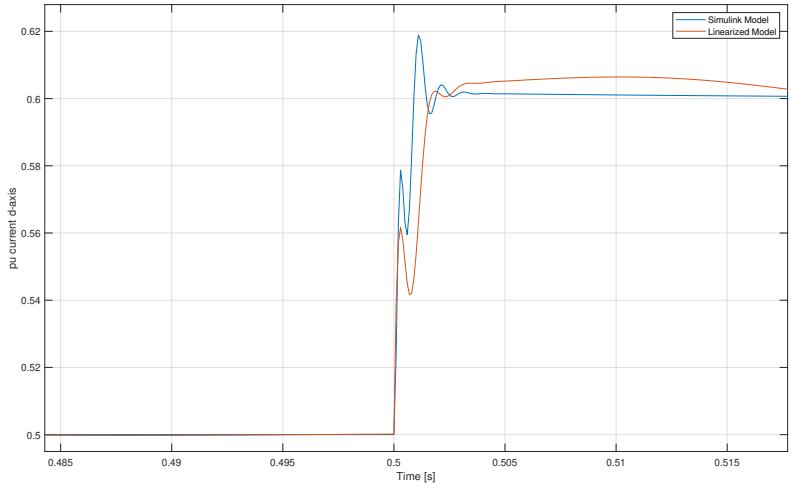

Figure 5.2: Comparison of detailed Simulink model and linearized model during transient state

5.1.1 Removing active damping

By setting the active damping constant $k_{ad} = 0$ and linearizing the model with $i_{cv}^{*,d} = 0.5$, it can be seen from Figure 5.3 that the oscillations disappear. The transient period can be seen in Figure 5.4. The detailed model does not have the same quick dampening of the oscillations when the active damping has been removed.

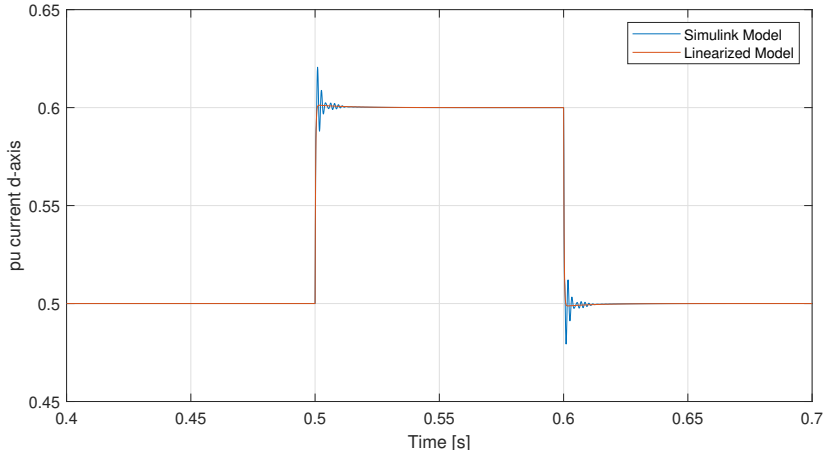

Figure 5.3: Comparison of detailed Simulink model and linearized model with no active damping of voltage

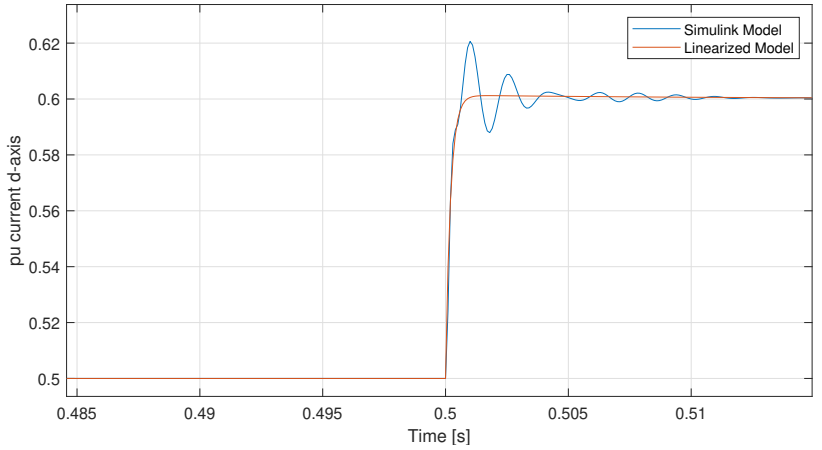

Figure 5.4: Comparison of detailed Simulink model and linearized model with no active damping of voltage during transient period

5.2 Linearization around different equilibrium points

To see if the linearized model will change much for different linearization points, the system is linearized around different input values of $i_{cv}^{*,d}$. The system has been linearized with a current reference in the d axis sweeping from a value of -1 to 1 pu. This corresponds to the full range of the BESS. In Figure 5.5 all eigenvalues of the system are shown. Figure 5.6 shows the eigenvalues that are close to the origin. The eigenvalues of the

linearized model do not change much for different linearization points for $i_{cv}^{*,d}$.

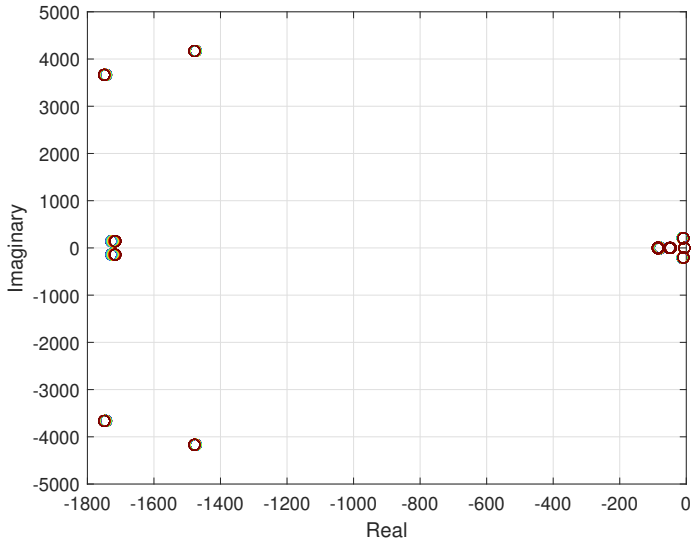

Figure 5.5: Eigenvalues of the linearized system. $i_{cv}^{*,d}$ sweeping from -1 to 1 pu from blue to red.

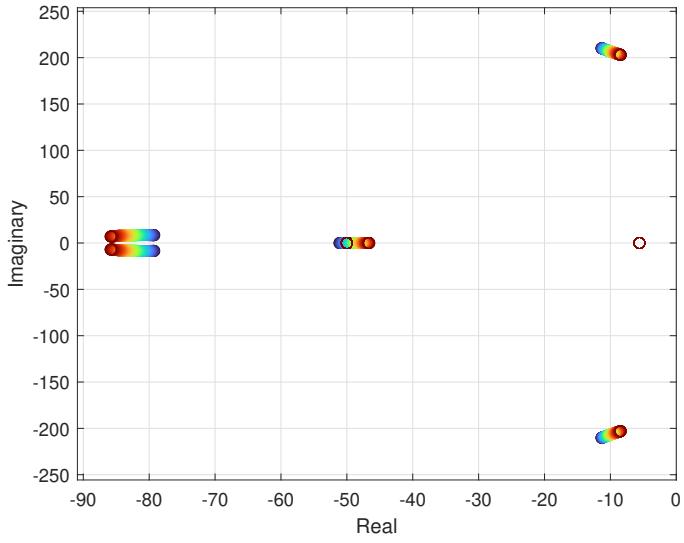

Figure 5.6: Eigenvalues of the linearized system close to the origin. $i_{cv}^{*,d}$ sweeping from -1 to 1 pu from blue to red.

6

Discussion

It can be seen from Figure 5.1 and Figure 5.2 that the linearized model does not accurately represent the detailed model in steady-state. There are oscillations in the linearized model that do not occur in the Simulink model. Because this occurs around the linearization point, where the model should be accurate, it will be necessary to go back to the modelling to see where the error is made.

A simulation of a linearized model of the active damping constant $k_{ad} = 0$ was tested. This resulted in the oscillations of the linear model being removed and it became a first-order response. The response of the linearized model still does not accurately represent the detailed model, so the fault may lie somewhere else. As Figure 5.4 shows, the detailed Simulink model also becomes more oscillating, meaning that removing the active damping is not a good solution for the final model.

It can be seen that the A-matrix in appendix C is mostly not dependent on the linearization point, meaning that the system matrix does not change much for different values of $i_{cv}^{*,d}$. This causes the eigenvalues of the linearized model to not change much, as seen in Figure 5.5 and Figure 5.6. The oscillation frequency of different linearization points will not vary much either because of the similar eigenvalues.

6.1 Further work

It is necessary to go over the linearized model to see what causes the deviation from the detailed Simulink model before doing further work that requires using the linearized model. When the linearized model has been properly verified, the outer control loops can be designed to achieve the control objective. The final control objective for the voltage support is to be defined in the master's thesis, along with suitable control strategies.

7

Conclusion

In this project thesis, a model of a voltage source converter to be used in combination with a battery energy storage system for voltage support in the distribution grid has been developed. This model was linearized around an equilibrium point and a verification of the linearized model was done against a detailed Simulink model. The verification analysis showed that the linear model does not accurately represent the detailed model, with oscillations in the linearized model that do not exist in the detailed model. This discrepancy needs to be further looked into. setting the active damping constant to zero yields no oscillations in the linearized model, but it also does not represent an accurate model of the system.

The linearized model's system matrices do not depend on many of the internal states, meaning that a change of reference current does not drastically alter the system matrices or their respective eigenvalues. This means that the oscillation found in the linear model does not disappear for a different linearization point.

The errors found in the linearized model must be found and a new verification of the model must be done before any further work using the linearized model is to be done.

Bibliography

[1] M. T. Lawder, B. Suthar, P. W. C. Northrop, S. De, C. M. Hoff, and O. Leitermann, "Battery energy storage system (bess) and battery management system (bms) for grid-scale applications." https://ieeexplore.ieee.org/stamp/stamp.jsp?tp=&arnumber=6811152, May 2014. (Accessed on 12/02/2022).

[2] K. Sand, K. Berg, A. Hammer, and K. Ingebrigtsen, "Veileder for kost/nytte-vurderinger ved integrasjon av batteri i distribusjonsnettet," 2020.

[3] J. Krata and T. K. Saha, "Real-time coordinated voltage support with battery energy storage in a distribution grid equipped with medium-scale pv generation," *IEEE Transactions on Smart Grid*, vol. 10, no. 3, pp. 3486–3497, 2019.

[4] E. Reihani, S. Sepasi, L. R. Roose, and M. Matsuura, "Energy management at the distribution grid using a battery energy storage system (bess)," *International Journal of Electrical Power & Energy Systems*, vol. 77, pp. 337–344, 2016.

[5] F. A. Viawan, "Voltage control and voltage stability of power distribution systems in the presence of distributed generation," 2008.

[6] S. Energi, "Planleggingsbok for kraftnett," 2011.

[7] O. og energidepartementet, "Forskrift om leveringskvalitet i kraftsystemet," January 2004.

[8] I. Madshaven, E. B. Mehammer, and J. Klemets, "Batteri som nettjeneste," 2022.

[9] J. Klemets, "Bass - electrochemical battery for voltage support in distribution grid - sintef." https://www.sintef.no/en/projects/2021/bass-electrochemical-battery-for-voltage-support-in-distribution-grid/. (Accessed on 12/14/2022).

[10] C.-T. Chen, *Linear System Theory And Design*. Oxford University Press Inc, 1999.

[11] S. D'Arco, J. Beerten, and J. A. Suul, *Eigenvalue-based analysis of small-signal dynamics and stability in DC grids*. Academic Press, 2021.

[12] P. Kundur, *Power System Stability and Control*. McGrac Hill, 1994.

[13] H. Saadat, *Power System Analysis*. PSA Publishing, 2010.

[14] K. Sharifabadi, L. Harnefors, H.-P. Nee, S. Norrga, and R. Teodorescu, *Design, Control, and Application of Modular Multilevel Converters for HVDC Transmission Systems*. John Wiley & Sons, 2016".

[15] N. Mohan, T. M. Undeland, and W. P. Robbins, *Power Electronics – Converters, Applications and Design*. John Wiley & Sons, 3 ed., 2003.

[16] R. Teodorescu, M. Liserre, and P. Rodriguez, *Grid Converters for Photovoltaic and Wind Power Systems*. John Wiley & Sons, 2011.

[17] S. D'Arco, J. A. Suul, and M. Molinas, "Implementation and analysis of a control scheme for damping of oscillations in vsc-based hvdc grids," in *2014 16th International Power Electronics and Motion Control Conference and Exposition*, pp. 586–593, 2014.

[18] J. Suul, S. D'Arco, P. Rodriguez, and M. Molinas, "Impedance-compensated grid synchronisation for extending the stability range of weak grids with voltage source converters," *IET Generation, Transmission & Distribution*, vol. 10, 01 2016.

Appendix

A Subscripts and Superscripts

Sub-/superscript	Description
d	d-axis
q	q-axis
α	α-axis
β	β-axis
cv	VSC terminal/going out of VSC
o	Connection to distribution grid
f	filter
c	current controller
lp	low pass filter
pll	phase locked loop
ad	active damping
$*$	reference value
p	proportional gain
i	integral gain
b	base value
0	linearization point

Table 7.1: Explanation of subscripts and superscripts.

B Nonlinear Differential Equations

$$\frac{d}{dt}v_o^d = \frac{\omega_b}{c_f}i_{cv}^d - \frac{\omega_b}{c_f}i_o^d + \omega_g\omega_b v_o^q \tag{7.1}$$

$$\frac{d}{dt}v_o^q = \frac{\omega_b}{c_f}i_{cv}^q - \frac{\omega_b}{c_f}i_o^q - \omega_g\omega_b v_o^d \tag{7.2}$$

$$\begin{aligned}\frac{d}{dt}i_{cv}^d = &\frac{\omega_b \cdot k_{p,c}}{l_f}i_{cv}^{*,d} - \frac{\omega_b \cdot k_{p,c}}{l_f}i_{cv}^d - \frac{\omega_b \cdot r_f}{l_f}i_{cv}^d + \frac{\omega_b \cdot k_{i,c}}{l_f}\gamma^d - \frac{\omega_b \cdot k_{ad}}{l_f}v_o^d \\ &+\frac{\omega_b \cdot k_{ad}}{l_f}\varphi^d - \omega_b \cdot k_{i,pll} \cdot \epsilon_{pll} \cdot i_{cv}^q - \omega_b \cdot k_{p,pll} \cdot \arctan\left(\frac{v_{pll}^q}{v_{pll}^d}\right) i_{cv}^q\end{aligned} \tag{7.3}$$

$$\begin{aligned}\frac{d}{dt}i_{cv}^q = &\frac{\omega_b \cdot k_{p,c}}{l_f}i_{cv}^{*,q} - \frac{\omega_b \cdot k_{p,c}}{l_f}i_{cv}^q - \frac{\omega_b \cdot r_f}{l_f}i_{cv}^q + \frac{\omega_b \cdot k_{i,c}}{l_f}\gamma^q - \frac{\omega_b \cdot k_{ad}}{l_f}v_o^q \\ &+\frac{\omega_b \cdot k_{ad}}{l_f}\varphi^q + \omega_b \cdot k_{i,pll} \cdot \epsilon_{pll} \cdot i_{cv}^d + \omega_b \cdot k_{p,pll} \cdot \arctan\left(\frac{v_{pll}^q}{v_{pll}^d}\right) i_{cv}^d\end{aligned} \tag{7.4}$$

$$\frac{d}{dt}\gamma^d = i_{cv}^{*,d} - i_{cv}^d \tag{7.5}$$

$$\frac{d}{dt}\gamma^q = i_{cv}^{*,q} - i_{cv}^q \tag{7.6}$$

$$\frac{d}{dt}i_o^d = \frac{\omega_b}{l_g}v_o^d - \frac{\omega_b \cdot r_g}{l_g}i_o^d + \omega_g \cdot \omega_b \cdot i_o^q - \frac{\omega_b \cdot \cos\left(\delta\theta_{pll}\right)}{l_g}\hat{v}_g \tag{7.7}$$

$$\frac{d}{dt}i_o^q = \frac{\omega_b}{l_g}v_o^q - \frac{\omega_b \cdot r_g}{l_g}i_o^q - \omega_g \cdot \omega_b \cdot i_o^d + \frac{\omega_b \cdot \sin\left(\delta\theta_{pll}\right)}{l_g}\hat{v}_g \tag{7.8}$$

$$\frac{d}{dt}\varphi^d = \omega_{ad} \cdot v_o^d - \omega_{ad} \cdot \varphi^d \tag{7.9}$$

$$\frac{d}{dt}\varphi^q = \omega_{ad} \cdot v_o^q - \omega_{ad} \cdot \varphi^q \tag{7.10}$$

$$\frac{d}{dt}v_{pll}^d = \omega_{lp,pll} \cdot v_o^d - \omega_{lp,pll} \cdot v_{pll}^d \tag{7.11}$$

$$\frac{d}{dt}v_{pll}^q = \omega_{lp,pll} \cdot v_o^q - \omega_{lp,pll} \cdot v_{pll}^q \tag{7.12}$$

$$\frac{d}{dt}\varepsilon_{pll} = \arctan\left(\frac{v_{pll,q}}{v_{pll,d}}\right) \tag{7.13}$$

$$\frac{d}{dt}\delta\theta_{pll} = \omega_b \cdot k_{p,pll} \cdot \arctan\left(\frac{v_{pll}^q}{v_{pll}^d}\right) + \omega_b \cdot k_{i,pll} \cdot \epsilon_{pll} \tag{7.14}$$

C Linear Small-Signal Matrices

$$A = \begin{bmatrix}
0 & \omega_b \cdot \omega_g & \frac{\omega_b}{c_f} & 0 & 0 & 0 & -\frac{\omega_b}{c_f} & 0 & 0 & 0 & 0 & 0 & 0 & 0 \\
-\omega_b \cdot \omega_g & \cos\theta & 0 & 0 & \frac{\omega_b}{c_f} & 0 & 0 & -\frac{\omega_b}{c_f} & 0 & 0 & 0 & 0 & 0 & 0 \\
-\omega_b \frac{k_{ad}}{l_f} & 0 & -\omega_b \frac{k_{p,c}+r_f}{l_f} & 0 & \frac{\omega_b \cdot k_{i,c}}{l_f} & 0 & 0 & 0 & \frac{\omega_b \cdot k_{ad}}{l_f} & 0 & 0 & -\omega_b \frac{k_{p,pll}}{v_{o,0}^d} i_{cv,0}^q & -\omega_b \cdot k_{i,pll} \cdot i_{cv,0}^q & 0 \\
0 & -\frac{\omega_b \cdot k_{ad}}{l_f} & 0 & -\omega_b \frac{k_{p,c}+r_f}{l_f} & 0 & \omega_b \frac{k_{i,c}}{l_f} & 0 & 0 & 0 & \omega_b \frac{k_{ad}}{l_f} & 0 & \omega_b \frac{k_{p,pll}}{v_{o,0}^d} i_{cv,0}^d & \omega_b \cdot k_{i,pll} \cdot i_{cv,0}^d & 0 \\
0 & 0 & -1 & 0 & 0 & 0 & 0 & 0 & 0 & 0 & 0 & 0 & 0 & 0 \\
0 & 0 & 0 & -1 & 0 & 0 & 0 & 0 & 0 & 0 & 0 & 0 & 0 & 0 \\
\frac{\omega_b}{l_g} & 0 & 0 & 0 & 0 & 0 & -\omega_b \frac{r_g}{l_g} & \omega_b \cdot \omega_{g,0} & 0 & 0 & 0 & 0 & 0 & \omega_b \frac{\sin \delta\theta_{pll,0}}{l_g} \hat{v}_{g,0} \\
0 & \frac{\omega_b}{l_g} & 0 & 0 & 0 & 0 & -\omega_b \cdot \omega_{g,0} & -\omega_b \frac{r_g}{l_g} & 0 & 0 & 0 & 0 & 0 & \omega_b \frac{\cos \delta\theta_{pll,0}}{l_g} \hat{v}_{g,0} \\
\omega_{ad} & 0 & 0 & 0 & 0 & 0 & 0 & 0 & -\omega_{ad} & 0 & 0 & 0 & 0 & 0 \\
0 & \omega_{ad} & 0 & 0 & 0 & 0 & 0 & 0 & 0 & -\omega_{ad} & 0 & 0 & 0 & 0 \\
\omega_{lp,pll} & 0 & 0 & 0 & 0 & 0 & 0 & 0 & 0 & 0 & -\omega_{lp,pll} & 0 & 0 & 0 \\
0 & \omega_{lp,pll} & 0 & 0 & 0 & 0 & 0 & 0 & 0 & 0 & 0 & -\omega_{lp,pll} & 0 & 0 \\
0 & 0 & 0 & 0 & 0 & 0 & 0 & 0 & 0 & 0 & 0 & \frac{1}{v_{o,0}^d} & 0 & 0 \\
0 & 0 & 0 & 0 & 0 & 0 & 0 & 0 & 0 & 0 & 0 & \omega_b \frac{k_{p,pll}}{v_{o,0}^d} & \omega_b \cdot k_{i,pll} & 0
\end{bmatrix}$$

$$
B = \begin{bmatrix}
0 & 0 & 0 & \omega_b v_{o,0}^q \\
0 & 0 & 0 & \omega_b v_{o,0}^d \\
\omega_b \frac{v_c}{l_f} & 0 & 0 & 0 \\
0 & \omega_b \frac{v_c}{l_f} & 0 & 0 \\
0 & 0 & 0 & 0 \\
0 & 1 & 0 & 0 \\
0 & 0 & -\omega_b \frac{\cos \delta \theta_{pll,0}}{l_g} & \omega_b \cdot i_{o,0}^q \\
0 & 0 & \omega_b \frac{\sin \delta \theta_{pll,0}}{l_g} & \omega_b \cdot i_{o,0}^d \\
0 & 0 & 0 & 0 \\
0 & 0 & 0 & 0 \\
0 & 0 & 0 & 0 \\
0 & 0 & 0 & 0 \\
0 & 0 & 0 & 0 \\
0 & 0 & 0 & 0
\end{bmatrix}
$$